Astron. Astrophys. 321, 177–188 (1997)

ASTRONOMY
AND
ASTROPHYSICS

Magnetic loops on rapidly rotating stars

Y.C. Unruh and M. Jardine

School of Physics & Astronomy, University of St. Andrews, North Haugh, St. Andrews, KY16 9SS, UK

Received 9 May 1996 / Accepted 19 September 1996

Abstract. We present models for the thermal and mechanical equilibria of slender magnetic loops on rapidly-rotating stars. These loops are embedded within an arcade located on the stellar equator. The loop properties are governed principally by the specified base pressure and conductive flux. While rapid rotation is important in determining the pressure structure within the loop, its main effect on the loop shape is through its influence on the base values of magnetic field strength, pressure, and conductive flux. We have compared our models with observations of the temperatures and X-ray fluxes of stars with a range of rotation rates. By using the observed variation of the differential emission measure with rotation rate Ω and allowing the base magnetic field strength to scale as $B \propto \Omega^q$ ($q = 0.5, 0.75, 1.0$) we can explain the variation of the temperature and X-ray flux of the slower rotators. For the most rapid rotators, however (approximately $\Omega/\Omega_\odot > 10$) it appears that a single value of q for all rotation rates cannot explain the observations and some other mechanism is needed to explain the saturation in the X-ray flux. We have also investigated the effect of using a heating function that is proportional to the density and one that falls off exponentially with height. With the parameters that we can calculate from these models it is not possible to discriminate between these two types of heating.

Key words: MHD – stars: magnetic fields – stars: coronae

1. Introduction

The magnetic structure of stellar coronae has become of increasing interest recently, since observations of magnetically-active stars have shown that the surface fields at least are organised into areas of spots (Stauffer & Hartmann 1987; Baliunas 1991; O'Dell & Collier Cameron 1993; Baliunas et al. 1995). The role of the magnetic field in governing the rotational spin-down of young stars through the action of a hot, magnetically-channelled wind makes it even more important to understand how the coronal field is structured, since angular momentum loss happens principally along open field lines. Areas of the stellar surface that are covered in closed loops are not believed to contribute significantly. Hence the fraction of the surface at any given rotation rate that is covered in closed field is relevant to the spin-down of the star. The extent of this "dead zone" was examined by Mestel & Spruit (1987) for a simple configuration with a dipole field at the stellar equator and open field at the poles. They found that the extent of the closed-field region increases with the strength of the dynamo-generated magnetic field, but decreases if the rotation rate is so high that centrifugal forces affect the pressure balance significantly. In reality, the magnetic structures will be more complex than this. Observations of stellar prominences now show that on a number of rapidly-rotating stars, closed field regions in which prominences are embedded extend out well into the stellar corona, filling a significant fraction of the coronal volume. These prominences form preferentially at the co-rotation radius (where centrifugal forces balance gravity) and move outwards over several days (see for example Jeffries 1993; Collier Cameron & Woods 1992 and references therein). Their contribution to the total angular momentum loss depends on the height above the surface at which the magnetic field can no longer support them and they are expelled.

In order to understand how the coronal field evolves, we need to examine the forces that govern the equilibria that are available to coronal loops. While finding an equilibrium does not guarantee that it will be stable, the absence of an equilibrium is an important constraint on the form of the magnetic field. In particular, we are interested in the role that rotation might play in determining the types of equilibria that are available at any given rotation rate. Jardine & Collier Cameron (1991) (hereafter [JC]) have calculated magnetostatic loop equilibria for an isothermal plasma on rotating stars. They showed that there is a maximum plasma pressure inside the loop beyond which no equilibrium exists. In their models, the maximum height of the loop depends mainly on the strength and scale of the external field within which the loop is embedded. For a dynamo-generated field, this is probably dependent on the rotation rate of the star. The effect of including an energy equation has also been investigated by Collier Cameron (1988). In these models, it is assumed that the loop shape is given by a dipole and the form of the cross-sectional loop area is prescribed as a function of distance along the loop. Here we consider loops that are em-

Send offprint requests to: Y.C. Unruh

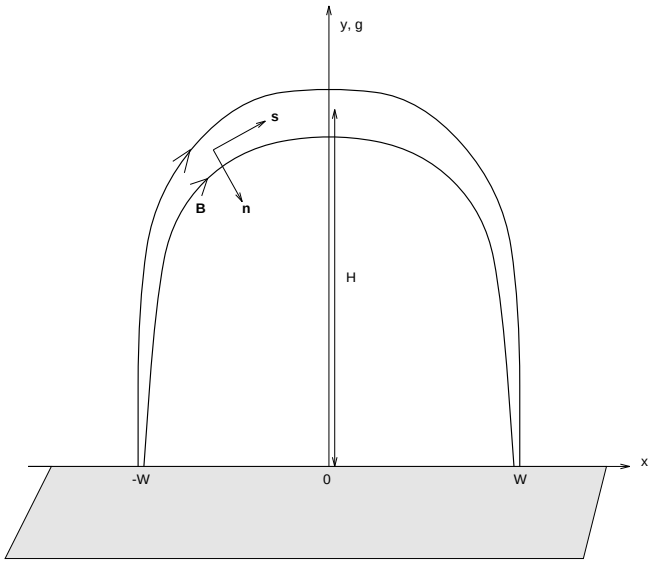

Fig. 1. The coordinate system and definitions for the loop.

bedded in an equatorial arcade and investigate the temperature and pressure structure inside these loops. We also look at the loop shapes and the maximum loop heights and widths.

2. Loop model

2.1. The coordinate system

Since we are principally interested in the vertical extent of closed loops, we model a region close to the equator, where the centrifugal force has the greatest effect on the loop height. For loops that emerge at higher latitudes, the centrifugal force no longer acts in the plane of the loop but tends to distort it, pulling it towards the equator. The effect of this distortion will be the subject of another paper. Here, we follow the setup and coordinate system chosen by [JC]. The loop lies along the x-direction and the y-axis points radially outwards (see Fig. 1). If the loop summit is at $x = 0$ and the foot points are at $(x, y) = (\pm W, 0)$, the vector along the magnetic field can be described by

$$\hat{\boldsymbol{s}} = \frac{1}{\sqrt{1 + X'^2}}(X', 1), \tag{1}$$

where $X' = dX(y)/dy$. The vector perpendicular to the field is given by

$$\hat{\boldsymbol{n}} = \frac{1}{\sqrt{1 + X'^2}}(1, -X'). \tag{2}$$

2.2. The equation of motion

The equation of motion for a plasma where fluid motions are much slower than the sound speed is given by:

$$-\boldsymbol{\nabla}\left(p + \frac{B^2}{2\mu}\right) + \frac{1}{\mu}(\boldsymbol{B}\cdot\boldsymbol{\nabla})\boldsymbol{B} + \rho\boldsymbol{g} = 0, \tag{3}$$

where p and ρ are the gas pressure and density. Here $\boldsymbol{g}$ combines the effect of gravity and the centrifugal force and is given by

$$\boldsymbol{g} = \left(-\frac{GM/R_*^2}{(\bar{y}+1)^2} + R_*\omega^2(\bar{y}+1)\right)\hat{\boldsymbol{y}}, \tag{4}$$

where $\bar{y}$ is the height (above the stellar surface) divided by the stellar radius. Along the field lines, i.e. in the direction of $\hat{\boldsymbol{s}}$, $\boldsymbol{j}\times\boldsymbol{B}$ vanishes so that the equation of motion reduces to

$$-\frac{dp}{ds} + \rho g_{\|} = 0, \tag{5}$$

where $g_{\|}$ is the component of $\boldsymbol{g}$ along the field lines. In the isothermal case this equation can be integrated to yield ([JC])

$$p = p_0\, e^{P(\bar{y})}, \tag{6}$$

where $P(\bar{y})$ is given by

$$P(\bar{y}) = \bar{y}\left(-\frac{\Phi_g}{\bar{y}+1} + \Phi_c(\bar{y}+2)\right). \tag{7}$$

Here, Φ_g and Φ_c are the surface ratios of the gravitational and centrifugal energies to the thermal energies, i.e.

$$\Phi_g = \frac{GM_*/R_*}{k_BT/m_H} \quad \text{and} \quad \Phi_c = \frac{\omega^2R_*^2/2}{k_BT/m_H}, \tag{8}$$

where k_B is the Boltzmann constant and m_H is the hydrogen mass.

Integrating the equation of motion over a pill-box that encompasses the boundary field line, one finds that the gas and magnetic pressure are conserved across the field lines, hence

$$B^2 + 2\mu p = \text{constant}. \tag{9}$$

Along $\hat{\boldsymbol{n}}$, the direction perpendicular to the field lines, the equation of motion becomes

$$X'(1+X'^2)\left[\frac{d}{dy}\left(p + \frac{B^2}{2\mu}\right) - \rho g\right] = -\frac{dX'}{dy}\frac{B^2}{\mu}. \tag{10}$$

This essentially describes the balance of forces due to magnetic tension (RHS), pressure and gravity.

2.3. Energy balance

The energy loss function is given by

$$\frac{\rho^\gamma}{\gamma-1}\frac{D}{Dt}\left(\frac{p}{\rho^\gamma}\right) = -\mathscr{L} = -\boldsymbol{\nabla}\boldsymbol{q} - L_{\rm r} + E_{\rm H}, \tag{11}$$

where $\boldsymbol{q}$ is the heat flux due to particle conduction, $\gamma = c_p/c_v$ is the ratio of the specific heats, and $L_{\rm r}$ denotes the radiative heat losses. We explore two different expressions for the sources of heating that have been collected together in $E_{\rm H}$. Firstly, $E_{\rm H} = (E_0/A)\, e^{-s/s_H}$, where s_H is the scale height in stellar radii and A is the loop cross-section. This allows us to vary the overall magnitude of the heating and its scale height. Secondly, we have

investigated heating functions that are proportional to the gas density.

For strong magnetic fields conduction works mainly along the field lines. We take the form developed by Spitzer (1962) for the conductive heat flux with

$$\boldsymbol{\nabla q} = \frac{dF_c}{ds} - \frac{F_c}{B}\frac{dB}{ds}, \tag{12}$$

where F_c is the conductive flux and is given by

$$F_c = -\alpha T^{5/2}\frac{dT}{ds}. \tag{13}$$

For a fully ionized plasma, α is of the order of 10^{-11} W m^{-1} K$^{-7/2}$. The radiative heat loss scales like $n_e^2\Lambda(T)$, where n_e is the electron density. For a fully ionized plasma this it is related to the temperature and pressure by $n_e = p/(2kT)$. $\Lambda(T)$ is taken from Rosner et al. (1978) who obtained a piecewise power-law fit to the loss function calculated by Raymont et al. (1976). For higher temperatures we use the extension given in Collier Cameron (1988).

In an adiabatic situation, the total change in heat is zero so that $\mathscr{S} = 0$. We can hence write

$$\frac{dF_c}{ds} = \frac{F_c}{B}\frac{dB}{ds} - \left(\frac{p}{2k_BT}\right)^2\Lambda(T) + E_{\rm H}. \tag{14}$$

3. Details of the model

We do not have any observational evidence for the detailed nature of the ambient field on these rapidly-rotating stars, although Doppler images suggest that the foot points of large spot complexes may be separated by about 60°. The effect of the ambient field on the nature of the flux tube is principally through the effect of pressure balance. The most important feature of the external field therefore is the rate at which its magnetic pressure falls off with height. A dipole field, while appropriate for studying the largest-scale structures, is less suitable for studying the smaller-scale fields closer to the stellar surface where we expect most of the X-ray emission to originate. In order to study a range of spatial scales therefore, we choose to model the ambient field as a potential arcade with $B_e^2 = B_0^2\,e^{-2ky}$. This allows us to change the scale-height of the external field simply by varying k. We have also investigated the effects of using a sheared arcade, but find that the results are qualitatively similar.

The presence of the flux tube will of course distort this arcade slightly as the flux tube pushes the arcade field lines out of the way. As we will show later, this distortion becomes significant when $\beta > 1$. We ignore this effect when calculating the loop equilibrium, but calculate *a posteriori* the point at which it becomes important and reject solutions with large β values.

The tube can then be described by seven coupled first-order differential equations:

$$\frac{dX}{ds} = \frac{X'}{\sqrt{1+X'^2}} \tag{15}$$

$$\frac{dp_i}{ds} = \frac{m}{2k_B\sqrt{1+X'^2}}g\frac{p_i}{T_i} \tag{16}$$

$$\frac{dT_i}{ds} = -\frac{F_i}{\alpha T_i^{2.5}} \tag{17}$$

$$\frac{dB_i}{ds} = \left(\frac{\mu m g}{2k_B\sqrt{1+X'^2}}\left(\frac{p_e}{T_e} - \frac{p_i}{T_i}\right) - \frac{kB_e^2}{\sqrt{1+X'^2}}\right)\frac{1}{B_i} \tag{18}$$

$$\frac{dF_i}{ds} = \frac{dB_i}{ds}\frac{F_i}{B_i} + E_H - \left(\frac{p_i}{2k_BT_i}\right)^2\Lambda(T_i) \tag{19}$$

$$\frac{dX'}{ds} = -\frac{dB_i}{ds}\frac{X'(1+X'^2)}{B_i} \tag{20}$$

$$\frac{dy}{ds} = \frac{1}{\sqrt{1+X'^2}} \tag{21}$$

Eqs. (15) and (21) follow from the way we set up the coordinate system. Eqs. (17) and (19) are equivalent to Eqs. (13) and (14). Eq. (16) is the hydrostatic equation expressed in terms of s rather than y. Differentiating the equation describing the balance of the magnetic and gas pressure between the loop and the surrounding plasma, namely

$$B_i^2 + 2\mu p_i = B_e^2 + 2\mu p_e, \tag{22}$$

yields (18). Eq. (20) is a rewrite of Eq. (10).

3.1. The surrounding plasma

To calculate the shape of the flux tube one needs to know the pressure structure of the plasma in which the tube is embedded. The usual approach is to assume that the plasma is isothermal, so that Eqs. (6) to (8) are valid.

If, however, the energy equation is used to calculate the temperature structure of the loop, the temperature increases very strongly within a short distance from the foot points. This means that, compared to the isothermal surrounding plasma, the pressure changes in the loop are dampened due to the inverse temperature dependence in Eq. (16). This can lead to unphysical effects, especially for loops that are higher than the co-rotation radius, when the density and pressure of the surrounding arcade become too large relative to the loop and can no longer be balanced by magnetic tension (see Sect. 3.2).

There is no *a priori* reason why the heating mechanism in the loops should be different from the heating mechanism of the corona. It is hence desirable to relax the isothermal assumption and to include the temperature variation of the surrounding plasma. This can be done fairly straightforwardly if the simplifying assumption is made that the loop shape does not vary considerably from the arcade shape. Then the path difference between the loop and the arcade can be neglected and the temperature, energy and pressure equations for the arcade can be solved in the same way as for the loop.

As the assumption that the surrounding plasma is isothermal has been dropped, Eqs. (15) to (21) are supplemented by three additional equations:

$$\frac{dp_e}{ds} = -\sin(kX)\frac{m}{2k_B}g\frac{p_e}{T_e} \tag{23}$$

$$\frac{dT_e}{ds} = -\frac{F_e}{\alpha T_e^{2.5}} \tag{24}$$

$$\frac{dF_e}{ds} = k\sin(kX)\,F_e + E_H - \left(\frac{p_e}{2k_B T_e}\right)^2 \Lambda(T_e) \tag{25}$$

These correspond to Eqs. (16), (17) and (19), except that we can now use $dX/ds = \cos(kX)$ and $dy/ds = -\sin(kX)$, as the shape of the arcade is fixed by our choice of a potential two-dimensional field for B_e,

$$B_e^x = B_0 \cos(kX)\, e^{-ky} \tag{26}$$

$$B_e^y = -B_0 \sin(kX)\, e^{-ky}. \tag{27}$$

Note that because of the assumption of a potential field, the shape prescription will not be valid for large values of the plasma β.

3.2. The loop equilibrium

The loop shape is determined by the equilibrium of forces due to magnetic pressure, buoyancy and magnetic tension. The buoyancy term (which in the isothermal case is only a function of the pressure) is now a function of the temperature as well. Furthermore, it changes sign as the loop rises across the co-rotation radius. The effect on the loop shape can be seen by looking at the derivative of the magnetic field. From Eq. (18) we get

$$\begin{aligned} -\frac{dB_i}{ds}\sqrt{1+X'^2} &= \frac{1}{B_i}\left(kB_e^2 - \mu g(\rho_e - \rho_i)\right) \\ &= kB_i + \frac{2\mu}{B_i}\left(k(p_i - p_e) - \frac{g}{2}(\rho_e - \rho_i)\right) \\ &= B_i k(1+\delta). \end{aligned} \tag{28}$$

If $|\delta|$ is small compared to unity we just recover the potential field solution. So the loop shape will only differ from the arcade if $|\delta|$ becomes of the order of unity, or

$$|(p_e - p_i) + \frac{g}{2k}(\rho_e - \rho_i)| \simeq \frac{B_i^2}{2\mu}. \tag{29}$$

In ideal MHD the deviation of the flux tube from the arcade is discontinuous at the boundary of the flux tube. In reality, we expect the flux tube to be surrounded by a current sheet that would contribute to the heating. The shape of a hot and over-pressured loop is shown as an example in Fig. 2a. Also shown are different arcade field lines. The dashed line shows the arcade field line that has the same gradient at its foot points as the loop. The lowest arcade is the arcade with the same foot point separation as the loop. Note that there is no maximum height for the arcades.

In most cases, the pressure difference in Eq. (29) will be much larger than the density difference, even if the loop rises above the co-rotation radius. This indicates that the plasma β has to be of the order of one in order for the loop shape to deviate. The equation also shows why, for a surrounding isothermal plasma, the rapid pressure increase of the arcade plasma relative to the loop plasma demands an increasing field strength with loop length beyond a critical point. As the external pressure increases rapidly, δ becomes negative and starts to approach values of the order of unity. Eventually, the RHS of Eq. (28) becomes negative and B_i will have to increase.

3.3. The boundary values

To solve the set of Eqs. (15-21, 23-25), we need to specify ten boundary values. These are the internal and external pressures and temperatures, the external magnetic field, the conductive flux inside and outside the loop and the initial foot point position and gradient of the magnetic field line. We can specify most of the parameters at the foot points so that they agree with values that are observed in the solar upper chromosphere or that are inferred from observations of other stars. The value for the conductive flux is not so readily observed. A common choice is to set the conductive flux to zero at the loop foot points as well as at the loop summit (e.g. Rosner 1978). Alternatively, one can use the differential emission measure (DEM = $Tn_e^2(dT/ds)^{-1}$) to constrain the values for the conductive flux.

Using this system of equations, one also has to be careful with the initial choice of the value for the loop foot point separation and gradient, X and X'. In principle, both the equations describing the arcade and the equations governing the loop allow infinitely long loops. In fact, it appears that a natural choice for X' would be to set it to zero. At the loop summit, however, its value tends to infinity. In the case of the arcade this does not pose any real problems as the loop summit is well defined and the loop length is obtained through

$$s = \int_{X_0}^{X} \frac{1}{\cos ku}\,du = \frac{1}{k}\left[\ln\tan(\frac{ku}{2} + \frac{\pi}{4})\right]_{X_0}^{X}. \tag{30}$$

If we assume that the loop summit is located at $X = 0$ then the foot point separation, $2W$, is given by

$$2W = 2X_0 = \frac{2}{k}\arctan e^{-kL} - \frac{\pi}{2k}. \tag{31}$$

As the loop will only deviate very slightly from the arcade at the foot points, we can assume a length for the surrounding arcade and calculate the foot point separation and loop gradient of this arcade. These values are then used as starting points for the loop calculations.

Symmetry imposes a further constraint, namely that the heat gradient along $\hat{\boldsymbol{s}}$ and hence the conductive flux have to vanish at the loop summit. From this it may seem that the problem is over-determined, but we additionally have to fix the heating. The order of magnitude of the heating can be deduced from the X-ray luminosity of the target stars (see e.g. Collier Cameron 1988).

4. Numerical results

4.1. Method

We used a Runge-Kutta method (Press et al. 1986) to solve the system of dependent differential equations. For a given set of

initial values the equations were integrated until the loop flattened off; we required that the change in height dy/ds was less than 10^{-8}. We have employed two different approaches to find solutions to Eqs. (15-21, 23-25); in the first approach, we prescribe the length of the arcade and then adjust the heating until the conductive flux vanishes at the loop summit (we required to conductive flux to fall below 10^{-7} of the initial flux). Alternatively, we can specify the heating and then adjust the loop length until the conductive flux vanishes at the loop top. For some heating values there are two loop lengths that will have vanishing conductive flux at the summit. In this case, the solutions with the longer loop lengths will show a temperature inversion, i.e. the maximum temperature is reached below the loop summit.

We also calculated the value of $\beta = 2p\mu/B^2$ along the loop and rejected solutions with β much greater than unity.

4.2. Loop solutions

We find that there are two distinct families of boundary conditions that yield solutions with vanishing conductive flux at the loop summit. It is possible to start with either a high or a very low initial value for the conductive flux. This simply corresponds to setting the base of the loop at slightly different levels in the transition region. Starting with a high initial conductive flux is very similar to following the behaviour of the low-flux solution, once the flux maximum has been reached. For loops without temperature inversions, it is in fact easier to prescribe the conductive flux (as this is an observable quantity through the DEM) at the loop foot points and then to adjust the heating until a solution is reached where F_c vanishes at the loop summit.

We have investigated different parameterisations for the heating function. In the first approach we chose an exponential heating with $E = (E_0/A)e^{-s/s_H}$, where A could either vary as an inverse function of the magnetic field strength or could be kept fixed. In this case the loop and arcade summit temperatures will differ if either the value of E_0 differs in- and outside the loop, or, alternatively, if the conductive flux differs. If the heat ratio between the loop and the arcade are changed, one usually also has to adjust the ratio of the base pressures so that the conductive flux reaches zero at the loop and arcade summit. Note that even if A is kept constant along the loop, the shape variation is still included in the equation for the conductive flux (19) through the term $(F_i/B_i)(\mathrm{d}B_i/\mathrm{d}s) = F_i\,\mathrm{d}\ln B_i/\mathrm{d}s$ as the area of the loop varies proportionally to B_i^{-1}.

In the second approach we parameterised the heating as $E = E_0 n$. One slightly worrying aspect of this parameterisation is that the heating will start to increase outwards once the loop rises above the co-rotation radius and the gas density starts to increase. For either heating parameterisation we find that the loop shape depends mainly on the ratio between the loop and arcade pressure. In the following sections we describe the behaviour of over- and under-pressured loops.

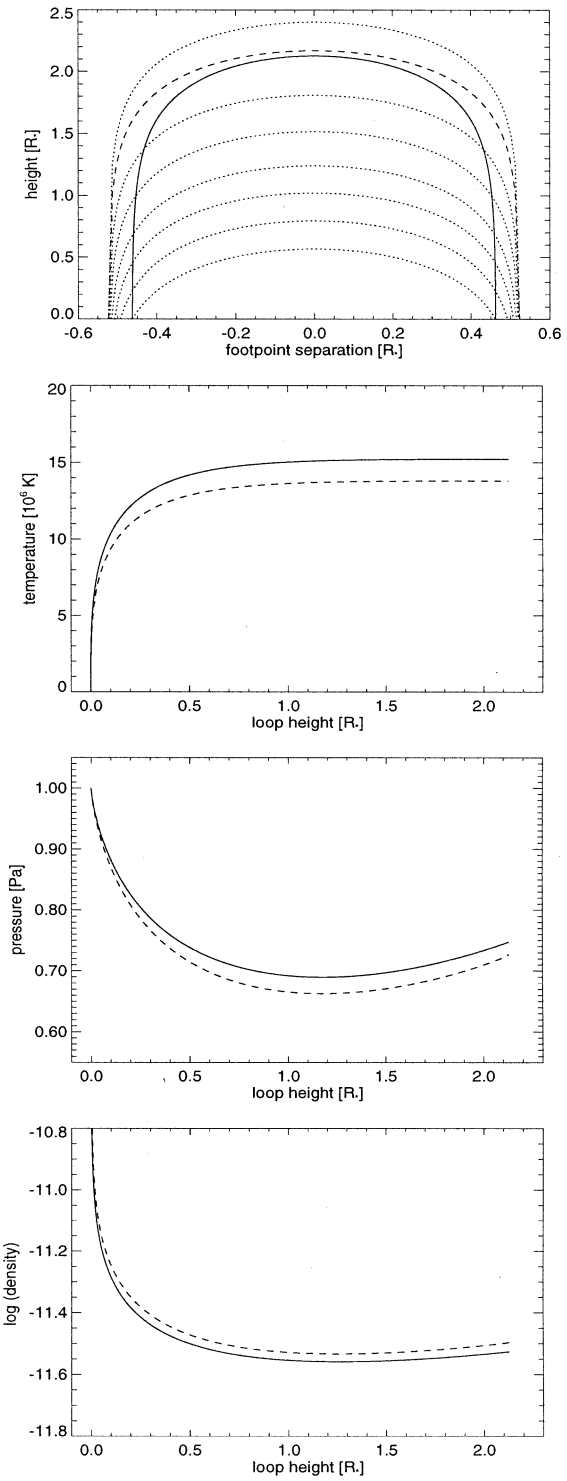

Fig. 2a–d. The shape (**a**), temperature (**b**), pressure (**c**) and density (**d**) of a typical hot and under-dense loop. The solid lines are for the loop, the dashed lines for the surrounding arcade. The star is assumed to rotate 70 times faster than the Sun and to have a field strength of 0.3 T. The loop has a length of 4.6 stellar radii. The dotted lines in **a** show arcade shapes for different foot point separations. The dashed line is the arcade field line that was used to calculated the external parameters.

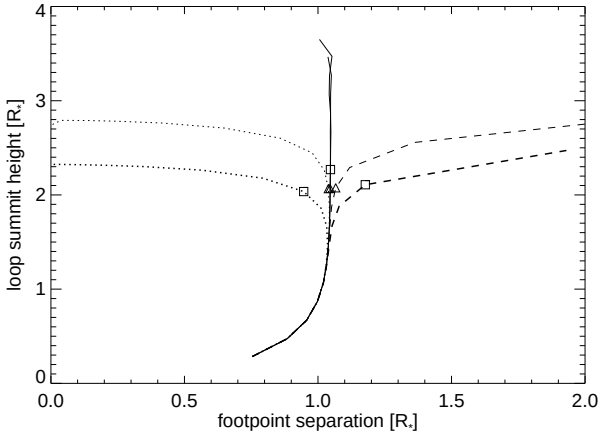

Fig. 3. The loop summit height as a function of foot point separation for heating that is proportional to the gas density. The dotted lines are for the over-pressured loops while the dashed lines are for the under-pressured and over-dense loops. The thick lines are for a star rotating with the same speed as the Sun and an external magnetic field of 0.02 T. The thin lines are for a star rotating with 50 times solar rotation rate ($B_e(0)$ = 1.0 T). We assume that the gas pressure scales with the square of the magnetic field and hence with the square of the rotation rate; the pressure is therefore 2500 times higher at the foot points of the rapid rotator than at the foot points of the slowly rotating star. The high-pressure (low-pressure) loops were produced by suppressing (enhancing) the conductive flux at the lower boundary by a factor of two. Solutions where β exceeds unity are marked by squares for the star with solar rotation rate and triangles for the rapid rotator.

4.3. Over-pressured hot loops

Loops that are hotter and have higher pressure than the surrounding arcade can be produced by increasing the conductive flux inside the loop. We generally find that the foot points of high-pressure loops come closer together when the loop starts to deviate from the arcade shape. This is because the magnetic tension needs to increase in order to contain the loop as β, the ratio between the gas and magnetic pressure, increases. This increase in the magnetic tension is achieved by decreasing the loop foot point separation. Thus, in Figs. 3 and 4 the curves on the left-hand side of the diagram are for the over-pressured loops.

Under-dense loops: These can arise with either heating parameterisation, but only when one deals with large temperature gradients. For low temperature gradients, the difference in loop and arcade summit temperature is not large enough to offset the pressure difference and one tends to get loops with an under-dense region close to the foot points where the temperature gradient is very large and a denser loop summit.

For high temperature gradients (i.e. large initial conductive flux values), the temperature difference at the loop summit becomes so large that the gas in the loops is less dense than in the arcade along the whole length of the loop. Fig. 2 shows the shape, temperature, pressure and density for a typical hot and over-pressured loop with high conductive flux at the base. It was obtained by increasing the base conductive flux inside the loop by a factor of 1.5 with respect to the base flux in the arcade.

If there is no pressure difference between the loop and arcade foot points and if the star rotates rapidly enough with loops that rise above the co-rotation radius, there is usually a height above which the external pressure becomes larger than the internal pressure. This happens in particular if the temperature in the loop is much higher than in the arcade, so that the pressure rise in the loop is dampened much more than the pressure rise in the arcade. At the pressure cross-over, the pressure difference in δ (see Eq. (29)) can for a while become less important than the density difference, so that there is a range of loop lengths and field strengths where over-pressured loops have larger foot point separations than the arcade.

The dotted lines in Fig. 3 show the loop summit height as a function of foot point separation for high-pressure and under-dense loops on a star with solar and 50 times solar rotation rate. The solid lines are for loops that have the same initial conductive flux, pressure and temperature as the arcade.

Over-dense loops: If we start off with a higher base pressure inside the loop, the resulting loop will usually be denser than the arcade everywhere. For an over-dense loop, the pressure and density terms in Eq. (29) have opposite signs below the co-rotation radius, but the density term will never be strong enough to offset the effects of the pressure difference. The foot points of hotter, and more importantly, over-pressured loops will therefore be closer together than for the arcade.

The dotted line in Fig. 4 shows the way an over-dense and over-pressured loop will be deformed as for a star with solar and 50 times solar rotation. The solid lines show the summit height for loops with the same base pressure and heating as the arcade. Whereas the heating was proportional to the gas density in Fig. 3, we used an exponential heating law for Fig. 4. Comparing the thicker lines (i.e. solar rotation) in the two figures shows that the heating parameterisation only has very little effect. The differences between the loop heights of the faster rotator are not due to the heating but to the fact that the over-pressured loops in Fig. 4 are also over-dense whereas the over-pressured loops in Fig. 3 are under-dense (see Sect. 4.6).

4.4. Over-pressured cool loops

A cool high-pressure loop is formed when the loop pressure is enhanced and the conductive flux is suppressed. Due to their higher pressures, the foot point separations of these loops usually decrease as they rise. In some cases, however, the higher conductive flux in the arcade and the resulting temperature increase can lead to a slower pressure fall-off in the arcade until the external pressure exceeds the internal pressure. This means that the loop foot points can be overpressured and the loop summit underpressured compared to the surrounding plasma. In these cases the foot point separations will increase as the loops rise.

4.5. Under-pressured and hot loops

Under-pressured loops tend to show increasing foot point separation as they rise and as the relative importance of the magnetic field decreases. Under-pressured and hot loops are just the opposite of the over-pressured cool loops described in 4.4. They are produced when the base pressure in the loop is suppressed with respect to the arcade pressure and when the conductive flux is enhanced. Again, we can get a pressure cross-over when the higher loop temperature slows the pressure fall-off in the loop sufficiently so that the loop pressure can fall below the arcade pressure.

For over-pressured loops, however, the values for the summit height as a function of loop foot point separation should only be taken as rough guides. This is because we assume a potential magnetic field for the surrounding arcade. But the loop will only start to deviate from the arcade shape once β becomes of the order of unity inside the loop. For an under-pressured loop β will generally be larger on the outside, so that the assumption of a potential field for the surrounding plasma tends to break down before the loop starts to deviate from the arcade shape.

One interesting distinction between the over-pressured and under-pressured loops are their maximum summit heights. Over-pressured loops have a natural maximum loop height as B_i^2, which is given by $B_i^2 = B_e^2 + 2\mu(p_e - p_i)$, has to remain positive. For an over-pressured loop the internal field strength is always less than the external field strength and will finally reach zero when $B_e^2 = 2\mu(p_i - p_e)$. Note that this can only happen once β exceeds unity. Under-pressured loops in general have no such natural summit height, but for under-dense loops there is an additional constraint that follows from the requirement that dB_i/ds has to remain negative. This means that $(\rho_e - \rho_i)g/k < B_e^2/\mu$ has to hold (see Eq. (18)). This is a weaker constraint as $(\rho_e - \rho_i)g/2k$ is usually much smaller than $p_e - p_i$.

4.6. Under-pressured and cool loops

Plasma in hot under-pressured loops is always less dense than the surrounding plasma, but whether the plasma in cool and under-pressured loops is over- or under-dense depends on the ratio of the foot point pressures and on the temperature gradient.

Over-dense loops: Most loops with high but suppressed conductive flux values will be over-dense independent of the heating parameterisation. The loop summit height as a function of the foot point separation is shown in Fig. 3 (dashed line) for heating that is proportional to the gas density. Below the co-rotation radius, the pressure and density terms act in the same direction (see Eq. (29)). Above it, the density term changes sign and tries to bring the foot points closer together. As before, it is usually the pressure difference that decides the fate of the loop and in most cases, the loop foot point separation will increase. Very fast rotators are an exception to this, as there is a narrow range of loop lengths and magnetic field strengths where the buoyancy term is larger than the pressure difference and for which the loop foot points move together.

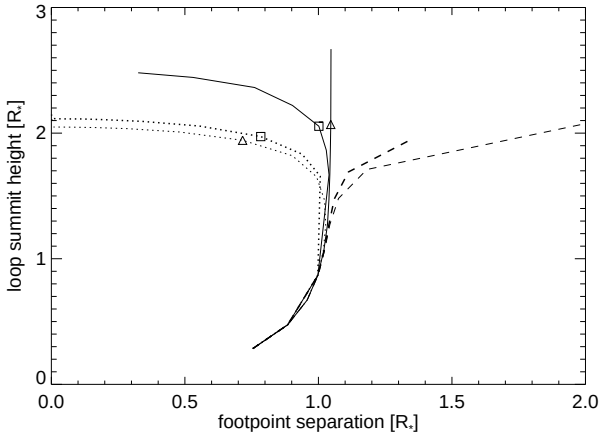

Fig. 4. The loop summit height as a function of foot point separation for exponential heating ($E = (E_0/A)e^{-s/s_H}$). The solid lines are for the case when the plasma inside and outside the loop has the same pressure and density structure. The dashed (dotted) lines show the loop summit height for under-pressured (over-pressured) loops; the solid lines are for loops that have the same foot point pressure and conductive flux as the arcade. The thin lines are for a star rotating 50 times faster than the Sun and a field strength of 1. T at the base, the thick lines for a star with solar rotation rate and field strength of 0.02 T. The squares and triangles indicate the parts of the loop from where β exceeds unity.

Under-dense loops: Cool and under-pressured loops where the gas at the summit is less dense than in the arcade tend to arise when the gas pressure at the base is higher in the arcade than in the loop. They can also occur when the gas pressure is the same at the loop and arcade base but the conductive flux in the loop is suppressed with respect to the arcade. In this case the resulting loops will always be cool and under-pressured, but only loops with comparatively low values of the base conductive flux will be under-dense.

For under-dense and under-pressured loops, the pressure and density difference act to pull the loops in opposite directions below the co-rotation radius, though the pressure term is usually orders of magnitude larger. Above the co-rotation radius, both terms act to pull the loop foot points apart. This is in contrast to what we observe in over-dense and under-pressured loops where the pressure and the density term counteract above the co-rotation radius.

The importance of Eq. (29) and the difference between the over-dense and under-dense loops can be seen clearly when comparing the loop heights for the fast rotator in Figs. 3 and 4. Whereas the loop heights for the solar rotation rate are similar on both figures, the maximum loop heights for the rapid rotator are of the order of 2.7 R_* in Fig. 3 and of the order of 2 R_* in Fig. 4. The loops in Fig. 3 can rise higher as the pressure and density terms have opposite signs once the loops reach above the co-rotation radius.

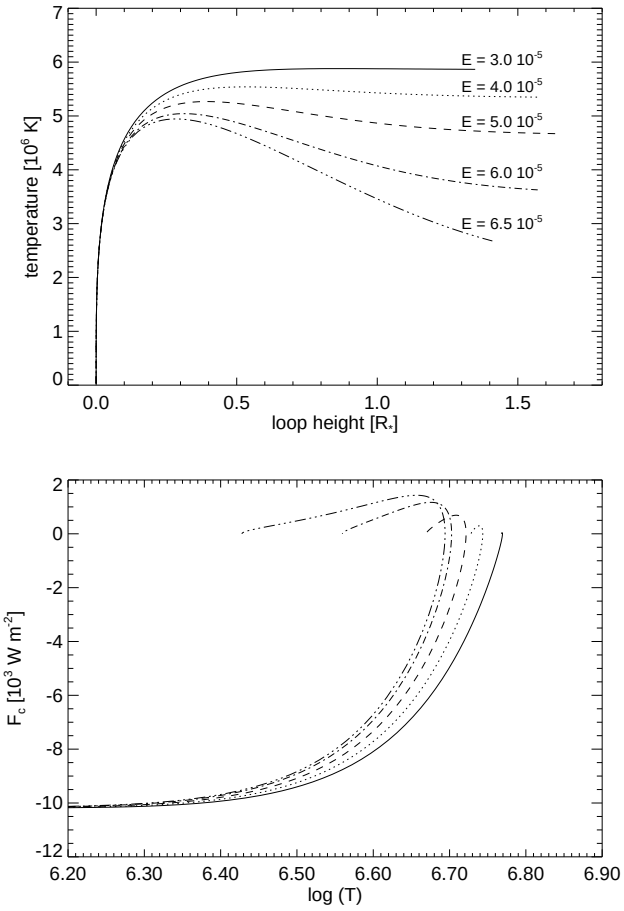

Fig. 5. The top figure shows the loop temperature along 5 loops with different initial heating values. The loops were produced with the exponential heating parameterisation. The bottom figure shows the conductive flux as a function of the loop temperature for the same loops. The heating constant is in units of W m^{-3}. All models are for a base pressure of 0.1 Pa, a rotation rate that is 50 times faster than the solar rotation rate, a magnetic scaling factor k = 3 and a conductive flux value of -10000 W m^{-2} at the base. Note that lower heating produces hotter loops.

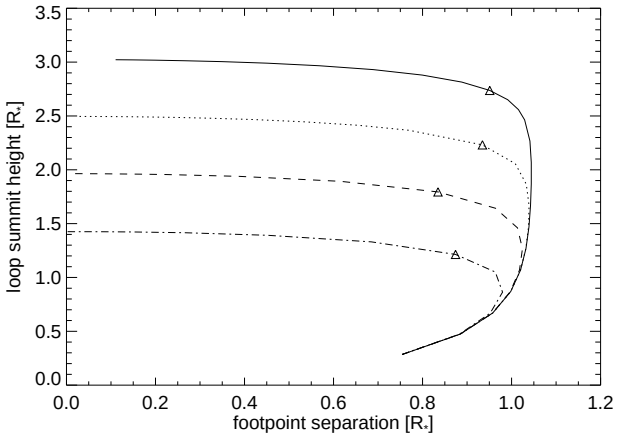

Fig. 6. The loop turn-off and maximum loop height for different magnetic field strengths. The scale factor for the magnetic field was fixed at k = 3. The initial values were $p_i(0)$ = 1 Pa, $p_e(0)$ = 0.8 Pa, $F_c(0)$ = 10^5 and T_i^0 = T_e^0 = 10^5K. The stellar rotation rate was 50 times the solar value. The different lines are (from top to bottom) for initial field strengths of 5 T, 1 T, 0.2 T and 0.04 T. The symbols give a rough indication from where on β exceeds unity at the loop summit.

4.7. The conductive flux and heating at the base

There is a threshold value for the conductive flux above which the loop summit temperature is almost uniquely defined by the conductive flux at the base. This threshold value is a function of the base pressure.

Below the threshold value, it is mainly the heating that determines the loop summit temperature. Maximum summit temperature is reached for very low heat input and, perhaps contrary to intuition, the loop summit temperature starts to fall as the heating is increased and we may get temperature inversions along the loop. Some examples are shown in Fig. 5.

Not all solutions with a temperature inversion are physical as the conductive flux can not always reach zero for a second time. This may be because of the expansion of the loop that is included in our model. The energetics for a variety of different loops, including some 'inverse-gravity' loops, have been discussed in detail in van den Oord & Zuccarello (1996). In agreement with these authors, we find that the minimum amount of heating required in order to obtain a solution where the conductive flux vanishes at the summit increases as the rotation rate increases, and that lower heating produces hotter loops.

4.8. The magnetic field strength and scale height

For a given magnetic field configuration and strength, the loops attain a maximum summit height. Fig. 6 shows the loop summit height as a function of the foot point separation for overpressured loops and four different values of B_0. At first the loop follows the arcade shape very closely, but as the ratio of the gas to the magnetic pressure increases, the magnetic tension has to increase so that the gas can be contained at the loop summit. The distance between the loop foot points therefore starts to decrease, though the loop summit height does not increase significantly. The turn-off point also depends strongly on the difference between the gas pressure inside and outside the loop. The larger the difference in gas pressures, the earlier the loop shape will deviate from the arcade shape.

We can also vary the value of k that determines the fall-off of the magnetic field. As k increases, the magnetic field strength falls off more rapidly and the loop summit height decreases. If shear is introduced ($B^2 = B_0^2\, e^{-2aky}$, where $a < 1$), the external field falls off less rapidly with height. The effect is therefore similar to lowering k without changing the foot point separation. The effects of varying the scale height on the maximum loop height are shown in Fig. 7.

As it is the ratio between the magnetic and the gas pressure that determines the loop height and the turn-off point, raising the gas pressure at the base has a similar effect as lowering the magnetic field strength in so far as the loop shape is concerned.

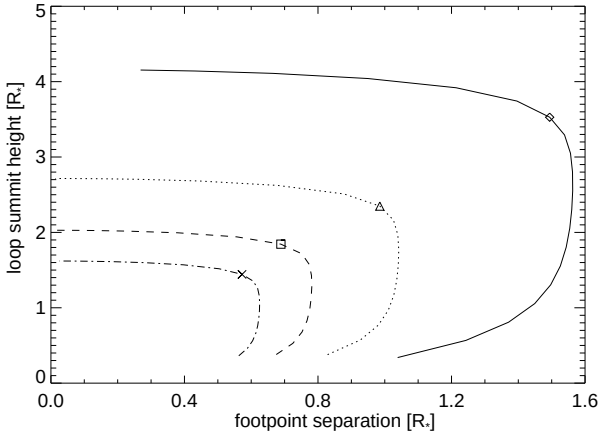

Fig. 7. The loop summit height as a function of foot point separation for different values of k. From top to bottom, k takes on the values from 2 to 5. The initial conditions are as in the previous figure with $B_e(0)$ = 1 T.

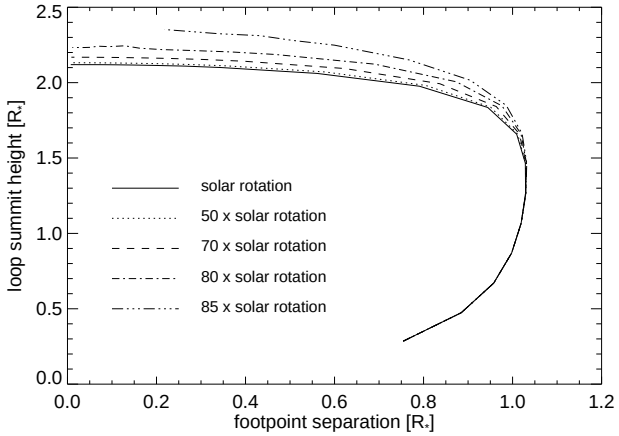

Fig. 8. The loop turn-off and maximum loop height for over- pressured and under-dense loops at different rotation rates. All curves are for $p_i(0)$ = $p_e(0)$ = 1 Pa, T_i^0 = T_e^0 = 10^5 K and B_e = 0.2 T. The conductive flux is twice as large at the loop base than at the arcade base.

The energetics of the loop, however, will be rather different. For fast rotators, the relative importance of the density term in Eq. (29) increases. Depending on whether the pressure and density terms have opposite signs above the co-rotation radius, the loop height either increases or decreases. Fig. 8 shows the effect of increasing the stellar rotation rate on the loop summit height for an over-pressured and under-dense loop. As the density term tries to counteract the effects of the pressure term above the co-rotation radius, the loop turnoff is delayed increasingly for higher rotation rates. The figure also shows that the influence of rotation is not very strong, so that we need to take into account two further effects: it is thought that the strength of the magnetic field increases with rotation rate, an effect that would allow the loops to rise higher. But if total pressure balance is maintained, the increase of the magnetic field might also go hand in hand with an increase in the base pressure, an effect that will shorten the loops.

For fast rotators, most length-dependent scaling relations (see eg. Rosner et al. 1978) break down. This is because the pressure scale height, and hence the pressure structure of the atmosphere, depends critically on the rotation velocity.

5. Importance of the rotational velocity

We can ask whether our model can predict coronal parameters for a range of rotation velocities that varies between the solar value and the much higher rotation rates that are observed on young and active stars. Jordan & Montesinos (1991) and Montesinos & Jordan (1993) have looked at the coronal temperatures and emission measures as a function of rotation rate. They find that the coronal temperature is proportional to the rotation rate, so that $\log T_c \propto \log \Omega$. They also found a relationship between temperature, gravity and emission measure (EM), $\log T_c \propto 3 \log(\mathrm{EM}/g)$.

Depending on the boundary conditions that we choose, our model agrees reasonably well with these scaling laws. In the following, we assume that the magnetic field strength scales with rotation rate, so $B \propto \Omega^q$. The most common choice is to set q = 1, but some observational results seem to indicate that the slope is somewhat flatter and q could be as low as 0.5 (Montesinos & Jordan 1993; Baliunas et al. 1996). Assuming equipartition, the gas pressure will then be proportional to the square of the rotation rate, $p \propto \Omega^{2q}$. If we set the loop foot points to a fixed temperature, the conductive flux is proportional to the square of the density (or pressure) divided by the differential emission measure (DEM). Fig. 9 shows the DEM of the C IV line as a function of rotation rate for single F, G and K stars. From this we deduce DEM $\propto \Omega^x$, with x about 1.5. The DEM in C IV is produced in a relatively narrow temperature range. We can hence use it to determine the scaling for the conductive flux at the base, F_c^0.

5.1. Results

We fixed the boundary conditions close to values observed on the Sun and then increased the rotation rate until we reached at least 50 times the solar value. For the first runs we assumed that q = 1, so that $B_e(0) \propto \Omega$, $p_i(0) \propto \Omega^2$ and $F_c(0) \propto \Omega^{4q-1.5} = \Omega^{2.5}$. The value for the initial temperature was kept fixed at 10^5 K. The advantage of setting the boundary temperature to 10^5 K is that we can use the C IV emission that is formed at this temperature to set the conductive flux value. The disadvantage is that one does not necessarily know whether the loop solutions are connected to the chromosphere (van den Oord & Zuccarello 1996). Also, one tends to underestimate the radiative losses and the total heat input required when starting with too high a value for the temperature at the loop foot point. We have compared the loop summit temperatures and pressures for loops with boundary temperatures of 10^5 K and 3×10^4 K (below which the gas becomes optically thick). We found no difference between the behaviour of the different loop solutions when we used the same

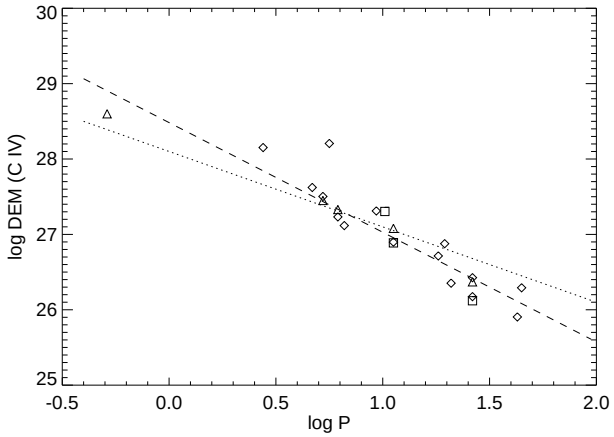

Fig. 9. The logarithm of the differential emission measure of C IV. The triangles are for data from Jordan et al. (1987), the squares are for data from Giampapa et al. (1985) and the diamonds are for data taken from Ayres et al. (1995). The DEM is measured in units of cm^{-5}, and the data from Ayres et al. (1995) and Giampapa et al. have been scaled by using measurements of stars that were also measured by Jordan *et al*. The star showing a very large value for the DEM at $\log P = 0.75$ is 110 Her; its rotation period has been deduced using its $v \sin i$ value and could be higher if it was viewed at a low inclination (Jordan & Montesinos 1991). The dashed line has a slope of –1.5 and corresponds to the linear least-square fit to the data excluding 110 Her. For comparison, the dotted line has a slope of –1.

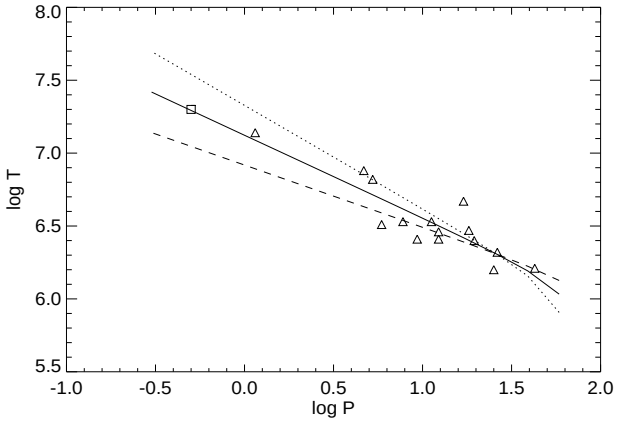

Fig. 10. Plot of the temperature versus period. The dotted line is for a model with $B_e(0) \propto \Omega$, $p_i(0) \propto \Omega^2$ and $F_c(0) \propto \Omega^{2.5}$. The solid line is for $B_e(0) \propto \Omega^{0.75}$, $p_i(0) \propto \Omega^{1.5}$ and $F_c(0) \propto \Omega^2$ and the dashed line for $B_e(0) \propto \Omega^{0.5}$, $p_i(0) \propto \Omega$ and $F_c(0) \propto \Omega^{1.5}$. The triangles are data from Jordan & Montesinos (1991); the square shows the coronal temperature and period for AB Dor.

scaling laws, except for a very small temperature and pressure offset.

For all runs, the loop length was fixed at $4R_*$ and the magnetic field fall-off was prescribed by setting $k = 3$. At each rotation rate, the base heating was adjusted until the conductive flux fell below a threshold value.

It turned out that the increase in temperature is too steep if the magnetic field is proportional to the rotation rate. As some observational results indicate that the dependence of the magnetic field on the rotation rate is indeed flatter, we also tried scaling laws with $q = 0.75$ and $q = 0.5$. For $q = 0.75$ we adopted $B_e(0) \propto \Omega^{0.75}$, $p_i(0) \propto \Omega^{1.5}$ and $F_c(0) \propto \Omega^2$; this assumes that the DEM of C IV depends linearly on the rotation rate (see the dotted line in Fig 9). For $q = 0.5$ we adopted $B_e(0) \propto \Omega^{0.5}$, $p_i(0) \propto \Omega$ and $F_c(0) \propto \Omega^{1.5}$. This is clearly not realistic in terms of the behaviour of the C IV DEM as a function of rotation rate.

Fig. 10 shows a plot of the summit temperature versus rotation rate for all three scaling laws. Clearly, the summit temperature for $B_e(0) \propto \Omega^{0.75}$ depicted by the solid line gives a much better fit than the linear dependence (dotted line) or a model where the magnetic field increases as the square root of the rotation rate (dashed line). The summit temperature is mainly a function of the conductive flux at the loop base. It is therefore not so much the behaviour of the magnetic flux as a function of rotation rate that determines the loop temperature, but the behaviour of the DEM. In fact, if we assume that the C IV DEM scales as $\Omega^{1.5}$ and $B_e(0) \propto \Omega^{0.75}$, we have to use $F_c(0) \propto \Omega^{1.5}$. The resulting temperature scaling then very much resembles the dashed line in Fig. 10 that was obtained for $B_e(0) \propto \Omega^{0.5}$, $p_i(0) \propto \Omega$ and $F_c(0) \propto \Omega^{1.5}$.

Table 1 lists the base heating, the summit temperature and pressure, the total heat deposited and the radiative losses a loop for heating that is proportional to the gas density.

Fig. 11 shows the X-ray flux as a function of period for a number of stars with $B - V > 0.6$ as listed in Hempelmann et al. (1995). The lines show the radiative losses in the loops. As in Fig. 10, the solid line is for $B_e(0) \propto \Omega^{0.75}$, the dotted line for $B_e(0) \propto \Omega$ and the dashed line for $B_e(0) \propto \Omega^{0.5}$. In general we find that our fits are slightly too flat for the slow rotators and fail to reproduce the flattening-off that is observed for the faster rotators. As the radiative loss is mainly a function of the square of the density, it is not very sensitive to any changes in the heating function. In Figs. 10 and 11, we have only plotted the temperature and the radiative losses for heating that is proportional to the density as the curves obtained with the other heating parameterisations coincide.

6. Summary and discussion

We have investigated the thermal and mechanical equilibria of magnetic loops on rapidly-rotating stars. These loops are assumed to be slender and are embedded in a potential arcade located on the stellar equator. We have analysed the effects of two different heating functions: one that is proportional to the density and one that falls off exponentially with height. While the total energy deposited in the loop depends on the form of heating function used, the summit temperature and pressure are largely unaffected, as are the radiative losses. As a result, it appears impossible to tell from present observations which heating mechanism is operating. The main factor governing the thermal properties of the loop solution is in fact the conductive flux at

Table 1. Initial and final values for the loops when the heating is proportional to the gas density. The magnetic field strength scales as $\Omega^{0.75}$.

Ω	B_0	p_0	$\log -F$	$\log E_0$	$\log T_s$	$\log p_s$	$\log E_{\rm tot}$	$\log L_r$
[$\Omega_\odot$]	[T]	[Pa]	[W m^{-2}]	[W m^{-3}]		[Pa]	[W m^{-2}]	[W m^{-2}]
.44	0.011	0.001	1.5	-5.6	6.03	-6.4	1.7	1.8
.67	0.015	0.002	1.8	-5.6	6.19	-5.2	1.6	2.0
1	0.020	0.004	2.2	-5.6	6.31	-4.3	1.7	2.2
1.5	0.027	0.007	2.5	-5.5	6.41	-3.7	1.8	2.4
2.3	0.037	0.013	2.9	-5.3	6.52	-3.1	2.0	2.6
3.4	0.050	0.024	3.2	-5.0	6.62	-2.6	2.3	2.9
5.1	0.067	0.043	3.6	-4.7	6.72	-2.1	2.6	3.1
7.6	0.091	0.079	3.9	-4.3	6.82	-1.7	3.0	3.4
11.4	0.124	0.146	4.3	-3.9	6.92	-1.3	3.3	3.7
17.1	0.168	0.268	4.6	-3.5	7.02	-0.9	3.7	4.0
25.6	0.228	0.493	5.0	-3.1	7.12	-0.6	4.1	4.3
38.4	0.309	0.905	5.4	-2.7	7.22	-0.3	4.4	4.5
57.7	0.418	1.663	5.7	-2.3	7.32	0.1	4.8	4.8
86.5	0.567	3.054	6.1	-1.9	7.42	0.4	5.1	5.2

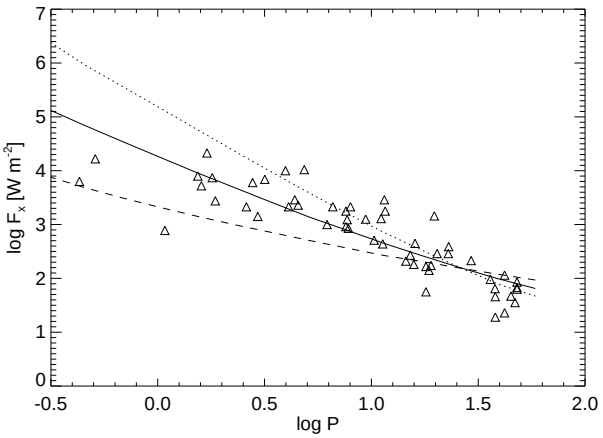

Fig. 11. The X-ray flux as a function of rotation rate for a number of stars taken from Hempelmann et al. (1995). Also plotted is the radiative loss in a loop. The dotted line is for a model with $B_e(0) \propto \Omega$, the dashed line for $B_e(0) \propto \Omega^{0.5}$ and the solid line for $B_e(0) \propto \Omega^{0.75}$. The X-ray flux is in units of W m^{-2}.

the base, which we impose as a boundary condition. The shape of the loop on the other hand depends mainly on the ratio of the internal and external plasma pressures, which again is imposed at the base of the loop.

Four different classes of solution have emerged from this study. These may be over- or under-pressured compared to their environment and either hotter or cooler. Looking at each case in turn we find the following.

- *Over-pressured, hot loops* can be produced if the base conductive flux or the heating is enhanced. As we look at progressively taller equilibria for these loops, the foot points first separate, reaching the maximum separation of the arcade, then come together again. These loops are generally over-dense, but under-dense cases can be found if a large base conductive flux is imposed, giving a large temperature gradient.
- *Over-pressured, cool loops* which are always over-dense can be produced if the base conductive flux or the heating is suppressed and the internal pressure is enhanced. The behaviour of the foot point separation is essentially as described above, i.e. the foot points first move apart then come together as the height is increased. Above the co-rotation radius, over-dense loops tend to be less tall than their under-pressured counterparts.
- *Under-pressured, cool loops* can be produced if the base conductive flux is suppressed. The higher conductive flux solutions tend to be over-dense, with foot points that separate with increasing loop height. The effect of very rapid rotation making the loop summit outwardly-buoyant can, however, cause the foot points to come together again. Under-dense solutions can be produced with lower conductive flux values. For these cases, the foot point separation increases with increasing loop height.
- *Under-pressured, hot loops* can arise when the base pressure in the loop is lower than in the arcade, though some solutions with low initial loop pressures show a pressure cross-over where the loop pressure will rise above the arcade pressure. The foot points of truly underpressured loops move apart as the loops rise; for loops with a pressure cross-over, the foot point separation tends to widen.

It is clearly possible to produce loops with a wide range of temperatures and structures, simply by adjusting their base values of heating, conductive flux or pressure. Since we have no reason to expect that a rapidly-rotating star will have a uniform surface, we might expect that the corona will be also be structured, both spatially and thermally. The results of the Mt. Wilson study (Baliunas et al. 1995) and Doppler imaging results (e.g. Unruh et al. 1995) show that many rapidly-rotating stars do indeed have starspots, and so have a highly-structured magnetic field at the surface. The discovery of stellar prominences (Collier Cameron & Robinson 1989) also demonstrates that the large-scale coronae of rapidly-rotating stars can also be

highly-structured, with closed magnetic loops extending out to several stellar radii.

While rotation can drastically alter the pressure stratification within a loop (which may be crucial for the formation of stellar prominences at the co-rotation radius), its influence on the loop shape is relatively modest if all other parameters are kept constant. Where rotation may have a very important effect, however, is in determining those very base conditions that characterise the thermal and mechanical properties of the loop. If we assume that the base magnetic field strength varies with rotation Ω as $B \propto \Omega^q$, then equipartition requires that $p \propto \Omega^{2q}$. On the basis of this alone we would expect that the nature of coronal loops should vary with rotation rate. The other critical factor in determining the loop behaviour is the conductive flux. We can use the observed values of the differential emission measure (DEM) for a sample of stars of known rotation rate to determine empirically how the conductive flux varies with rotation rate. We do this by looking at the DEM for the C IV line which is formed in a fairly narrow temperature range. At a constant temperature, the conductive flux is proportional to the square of the density (or pressure) divided by the DEM. We find from observations that DEM $\propto \Omega^x$ where x lies between 1 and 1.5, implying that the conductive flux F_c varies with rotation as $F_c \propto \Omega^{4q-x}$.

Using these scalings we have compared our models with the observed temperatures and X-ray fluxes of stars of differing rotation rates. We tried three prescriptions for the magnetic field variation: $q = 0.5, 0.75, 1.0$. The best fit to the observed temperatures is obtained with $q = 0.75$, which also gives a reasonable fit to the X-ray flux at least for the intermediate rotators. Whereas the radiative losses, loop summit temperature and summit pressure are very similar for all three heating parameterisations, the total heat deposited in the loop depends somewhat on the choice of the heating function. The heat deposited is not a measurable quantity, though, so that we cannot use this model to differentiate between the different heating mechanisms.

While our models can explain the variation with rotation rate in the temperature and X-ray flux from stellar coronae at low rotation rates, simply by allowing the magnetic field strength to scale with rotation, it is clear that some other mechanism is needed to explain the more rapid rotators. The saturation of the X-ray flux at high rotation rates has been known for some time and is often attributed to a change in behaviour of the dynamo (Vilhu & Rucinski 1983; Hempelmann et al. 1995).

There are two effects that could result in the saturation effect that is observed in the data. Firstly, equipartition (i.e. $p \propto B^2$) might not hold for the faster rotators, if e.g. the gas pressure cannot continue to increase as the magnetic field strength (or the packing of the loops) increases. Secondly, the dynamo could change configuration, so that the scaling ($B \propto \Omega^q$) of the magnetic field strength as a function of rotation rate changes. From our models, we see that reducing the value of q, which corresponds to a weaker dependence of the magnetic field strength on rotation rate, gives lower values for the X-ray flux. We have not pursued a model with variable q because of the lack of data on the C IV DEM at high rotation rates.

Acknowledgements. The authors would like to thank the referee, Dr. van den Oord, for very useful comments that helped to clear up some of the issues discussed. The authors would also like to thank Andrew Collier Cameron and Miguel Ferreira for useful discussions. MMJ acknowledges the support of a PPARC Advanced Fellowship during the course of this work. YCU would like to thank the Astrophysics Division at RAL for their hospitality and acknowledges the support through a PPARC funded PDRA during part of the work.

References

Ayres T. R. et al.., 1995, ApJS, 96, 223
Baliunas S. L. et al., 1995, ApJ, 438, 269
Baliunas S., Sokoloff D., Soon W., 1996, ApJ, 457, L99
Baliunas S. p. 809, The University of Arizona Press, Tucson, 1991
Collier Cameron A., Robinson R. D., 1989, MNRAS, 236, 57
Collier Cameron A., Woods J. A., 1992, MNRAS, 258, 360
Collier Cameron A., 1988, MNRAS, 233, 235
Giampapa M. S., Golub L., Peres G., Serio S., Vaiana G. S., 1985, ApJ, 289, 203
Hempelmann A., Schmitt J. H. M. M., Schultz M., Rüdiger G., Stępień K., 1995, A&A, 294, 515
Jardine M. M., Collier Cameron A., 1991, Solar Phys., 131, 269
Jeffries R. D., 1993, MNRAS, 262, 369
Jordan C., Montesinos B., 1991, MNRAS, 252, 21P
Jordan C., Ayres T. R., Brown A., Linsky J. L., Simon T., 1987, MNRAS, 225, 903
Mestel L., Spruit H. C., 1987, MNRAS, 226, 57
Montesinos B., Jordan C., 1993, MNRAS, 264, 900
O'Dell M. A., Collier Cameron A., 1993, MNRAS, 262, 521
Press W. H., Flannery B. P., Teukolsky S. A., Vetterling W. T., 1986, Numerical Recipes: The Art of Scientific Computing. Cambridge University Press, Cambridge
Raymond J. C., Cox D. P., Smith B. W., 1976, ApJ, 204, 290
Rosner R., Tucker W. H., Vaiana G. S., 1978, ApJ, 220, 643
Spitzer L., 1962, Physics of Fully Ionized Gases. Interscience, NY
Stauffer J. R., Hartmann L. W., 1987, ApJ, 318, 337
Unruh Y. C., Collier Cameron A., Cutispoto G., 1995, MNRAS, 277, 1145
van den Oord G. H. J., Zuccarello F., 1996, in Strassmeier K. G., Linsky J. L., eds, IAU Symp. 176, Stellar Surface Structure. Kluwer
Vilhu O., Rucinski S. M., 1983, A&A, 127, 5

This article was processed by the author using Springer-Verlag LaTeX A&A style file *L-AA* version 3.